

# A low-cost monitor for simultaneous measurement of fine particulate matter and aerosol optical depth – Part 3: Automation and design improvements

5 Eric A. Wendt<sup>1</sup>, Casey Quinn<sup>1</sup>, Christian L’Orange<sup>1</sup>, Daniel D. Miller-Lionberg<sup>3</sup>, Bonne Ford<sup>4</sup>, Jeffrey R. Pierce<sup>4</sup>, John Mehaffy<sup>1</sup>, Michael Cheeseman<sup>4</sup>, Shantanu H. Jathar<sup>1</sup>, David H. Hagan<sup>6</sup>, Zoey Rosen<sup>5</sup>, Marilee Long<sup>5</sup>, and John Volckens<sup>1,2</sup>

<sup>1</sup>Department of Mechanical Engineering, Colorado State University, Fort Collins, Colorado, USA, 80523

10 <sup>2</sup>Department of Environmental and Radiological Health Sciences, Colorado State University, Fort Collins, Colorado, USA, 80523

<sup>3</sup>Access Sensor Technologies, LLC, Fort Collins, Colorado, USA, 80523

<sup>4</sup>Department of Atmospheric Science, Colorado State University, Fort Collins, Colorado, USA, 80523

15 <sup>5</sup>Department of Journalism and Media Communication, Colorado State University, Fort Collins, Colorado, USA, 80523

<sup>6</sup>QuantAQ, Inc., Somerville, Massachusetts, USA, 02143

*Correspondence to:* John Volckens (john.volckens@colostate.edu)

## Abstract.

20 Atmospheric particulate matter smaller than 2.5 micrometers in diameter (PM<sub>2.5</sub>) has a negative impact on public health, the environment, and Earth’s climate. Consequently, a need exists for accurate, distributed measurements of surface-level PM<sub>2.5</sub> concentrations at a global scale. Existing PM<sub>2.5</sub> measurement infrastructure provides broad PM<sub>2.5</sub> sampling coverage, but does not adequately characterise community-level air pollution at high temporal resolution. This motivates the development of low-cost sensors which can be more practically deployed in spatial and temporal configurations currently lacking proper characterization. In part 1 of this series we described the development and validation of a first-generation device for low-cost measurement of AOD and PM<sub>2.5</sub>: The Aerosol Mass and Optical Depth (AMODv1) sampler. Part 2 of the series describes a citizen-science field deployment of the AMODv1 device. Here in part 3, we present an updated version of the AMOD, known as AMODv2, featuring design improvements and extended validation to address the limitations of the AMODv1 work. The AMODv2 measures AOD and PM<sub>2.5</sub> at 20-minute time intervals. The sampler includes a motorized sun-tracking system alongside a set of four optically filtered photodiodes for semi-continuous, multi-wavelength (current version at 440, 500, 675, and 870 nm) AOD sampling. Also included are a Plantower PMS5003 sensor for time-resolved optical PM<sub>2.5</sub> measurements and a

30

pump/cyclone system for time-integrated gravimetric filter measurements of particle mass and composition. AMODv2 samples are configured using a smartphone application and sample data are made available via data streaming to a companion website (csu-ceams.com). We present the results of a nine-day AOD validation campaign where AMODv2 units were co-located with an AERONET (Aerosol Robotics Network) instrument as the reference method at AOD levels ranging from  $0.02 \pm 0.01$  to  $1.59 \pm 0.01$ . We observed close agreement between AMODv2s and the reference instrument with mean absolute errors of 0.04, 0.06, 0.03, and 0.03 AOD units at 440 nm, 500 nm, 675 nm, and 870 nm, respectively. We derived empirical relationships relating the reference AOD level with AMODv2 instrument error and found that the mean absolute error in the AMODv2 deviated by less than 0.01 AOD units between clear days and elevated-AOD days and across all wavelengths. We identified bias from individual units, particularly due to calibration drift, as the primary source of error between AMODv2s and reference units. In a test of 15-month calibration stability performed on 16 AMOD units, we observed median changes to calibration constant values of -7.14%, -9.64%, -0.75%, and -2.80% at 440 nm, 500 nm, 675 nm, and 870 nm, respectively. We propose annual recalibration to mitigate potential errors from calibration drift. We conducted a trial deployment to assess the reliability and mechanical robustness of AMODv2 units. We found that 75% of attempted samples were successfully completed in rooftop laboratory testing. We identify several failure modes in the laboratory testing and describe design changes we have since implemented to reduce failures. We demonstrate that the AMODv2 is an accurate, stable and low-cost platform for air pollution measurement. We describe how the AMODv2 can be implemented in spatial citizen-science networks where reference-grade sensors are economically impractical and low-cost sensors lack accuracy and stability.

## 1 Introduction

Fine particulate matter air pollution (PM<sub>2.5</sub>) is a leading cause of human morbidity and mortality, and also a significant contributor to radiative climate forcing (Myhre et al., 2013; Forouzanfar et al., 2016; Brauer et al., 2016; Vohra et al., 2021). Inhaled PM<sub>2.5</sub> can penetrate deep into the lungs, leading to both acute and chronic health impacts (Pope and Dockery, 2006; Janssen et al., 2013; Feng et al., 2016; Kim et al., 2019). Each year, millions of deaths worldwide are attributed to PM<sub>2.5</sub> exposure (Brauer et al., 2016; Forouzanfar et al., 2016). In addition to public health, PM<sub>2.5</sub> also contributes to visual degradation of the atmosphere and affects the climate by influencing Earth's radiative budget (Myhre et al., 2013). Regions with the highest levels of air pollution often lack adequate ground level monitoring (Snider et al., 2015; Brauer et al., 2016). Thus, disease estimates for much of the world's population rely on exposure estimates where satellite data or model simulations are the best or only source of information on human exposure. Installing a global network of reference-grade surface monitors is not currently feasible due to the high installation and maintenance costs.

Satellite remote sensing, supplemented with data from surface measurements and chemical transport models (CTMs), represents the state-of-the-art for global PM<sub>2.5</sub> monitoring at relatively high temporal and spatial resolution (van Donkelaar et al., 2016, 2019; Hammer et al., 2020; Lee, 2020). Measurements from satellite instruments, such as the Moderate Resolution Imaging Spectrometer (MODIS) and the Multi-angle Imaging SpectroRadiometer (MISR) (Salomonson et al., 1989; Diner et al., 1998), are used to estimate surface-level PM<sub>2.5</sub>

concentrations (e.g. Liu et al., 2005), which in turn have facilitated research on the health effects associated with PM<sub>2.5</sub> exposure (Brauer et al., 2016; Forouzanfar et al., 2016; Li et al., 2018; Lu et al., 2019). Satellites equipped with aerosol remote sensing instrumentation retrieve aerosol optical depth (AOD), a measure of light extinction in the atmospheric column, which can then be converted to ground level PM<sub>2.5</sub> using a CTM or statistical relationship (Liu et al., 2005; van Donkelaar et al., 2006, 2010, 2012, 2016; Hammer et al., 2020). The relationship between AOD and PM<sub>2.5</sub> can be expressed as follows (Liu et al., 2005):

$$PM_{2.5} = \eta \cdot AOD \tag{1}$$

where  $\eta$  is a conversion factor between PM<sub>2.5</sub> and AOD. The uncertainty of surface-level PM<sub>2.5</sub> concentrations derived from satellite observations has two main components: 1) the uncertainty of the satellite AOD measurement and 2) the uncertainty of the modeled PM<sub>2.5</sub> to AOD ratio ( $\eta$ ) (e.g. Ford and Heald, 2016; Jin et al., 2019).

The error of the satellite AOD retrieval can be estimated using ground-level AOD measurements from instruments known as sun photometers (e.g., Sayer et al., 2012). The Aerosol Robotics Network (AERONET) provides reference-quality AOD measurements at hundreds of locations around the Earth; these data are used to constrain and reduce uncertainties in AOD values (Holben et al., 1998). AERONET instruments are rarely deployed at high spatial density (i.e. sub-city scale), outside of field campaigns (e.g. Garay et al., 2017), due to the high cost of the instrument and supporting equipment (>\$50,000). Determining the uncertainty in the modeled PM<sub>2.5</sub> to AOD ratio requires co-locating AOD and PM<sub>2.5</sub> measurements. The Surface PARTiculate mAtter Network (SPARTAN) was established to provide co-located PM<sub>2.5</sub> and AOD reference measurements and to evaluate uncertainties in both AOD and the PM<sub>2.5</sub> to AOD ratio; however, the number of SPARTAN sites worldwide is limited by number (~20 active sites), equipment, and operational costs (Snider et al., 2015).

Networks of low-cost nephelometers (notably the Plantower PMS5003), have been suggested and deployed in large numbers as a means to provide surface PM<sub>2.5</sub> data at a higher spatial density than can be achieved with reference-grade monitors (Lin et al., 2020; Li et al., 2020; Badura et al., 2020; Lu et al., 2021; Chadwick et al., 2021). However, low-cost sensors (or more specifically, the Plantower PMS5003 devices) tend to exhibit measurement bias (Kelly et al., 2017; Zheng et al., 2018; Levy Zamora et al., 2019; Sayahi et al., 2019; Tryner et al., 2020), requiring correction relative to reference monitors (Ford et al., 2019; Wendt et al., 2019). Low-cost Sun photometers have been deployed at high-spatial resolution to evaluate satellite AOD uncertainty as part of the Global Learning and Observations to Benefit the Environment (GLOBE) program (Boersma and de Vroom, 2006; Brooks and Mims, 2001). GLOBE Sun photometers were operated by students as part of education programming, resulting in over 400 measurements between January 2002 and October 2005 in the Netherlands (Boersma and de Vroom, 2006). These data were used to evaluate satellite-derived AOD in corresponding regions. However, the authors noted difficulty coordinating with schools to achieve consistent measurements, specifically those corresponding with satellite overpasses. Collectively, these previous efforts have advanced the understanding of AOD and PM<sub>2.5</sub>:AOD variability considerably. However, there is still demand for co-located PM<sub>2.5</sub> and AOD samplers deployed at higher spatial density and with greater temporal resolution (Ford and Heald, 2016; Garay et al., 2017; Jin et al., 2019). Samplers used in these networks must be sufficiently low-cost to deploy in large numbers, have manageable operational and maintenance requirements, and provide useful and reliable PM<sub>2.5</sub> and AOD

measurements (i.e., measurement data of sufficient accuracy and precision so as to support scientific inference or public decision-making). Thus, consideration should be given to the tradeoffs associated with deploying low-cost sensors such as scalability and simplicity versus accuracy and reliability.

In part 1 of this series of articles, we describe a low-cost, compact PM<sub>2.5</sub> and AOD ground monitor (Wendt et al., 2019; Ford et al., 2019). The device, known as the Aerosol Mass and Optical Depth (AMOD) sampler, featured a PM<sub>2.5</sub> cyclone inlet for integrated gravimetric sampling and composition analysis, a low-cost nephelometer (Plantower PMS5003, Beijing, China) for real-time PM<sub>2.5</sub> mass estimate, and four filtered-photodiode (Intor Inc., Socorro, NM, USA) sensors at 440, 520, 680, and 870 nm for measuring AOD. Here, we refer to this earlier instrument as the AMODv1. The assembly cost for the first manufacturing set of 25 AMODv1s was under \$1,100 per unit (Wendt et al., 2019). The results of a field validation campaign revealed agreement to within 10% (mean relative error) for AOD values relative to co-located AERONET instruments. The mean AOD difference was <0.01 with 95% confidence upper and lower limits of agreement of 0.03 and -0.02, respectively. With respect to PM<sub>2.5</sub>, the AMODv1 filter measurements agreed within 8% (mean relative error) relative to Federal Equivalent Method (FEM) monitors from the Environmental Protection Agency (EPA), with a mean difference of -0.004 μg m<sup>-3</sup> and 95% confidence upper and lower limits of agreement of 1.84 and -1.85 μg m<sup>-3</sup>, respectively (Wendt et al., 2019). With respect to real-time PMS5003 PM<sub>2.5</sub> measurements, the mean relative error between the AMODv1 and an FEM monitor was 1.98 μg m<sup>-3</sup> with a mean difference of 0.04 μg m<sup>-3</sup> and 95% confidence upper and lower limits of agreement of 5.02 and -4.95 μg m<sup>-3</sup>, respectively (Wendt et al., 2019). These results indicated that the AMODv1 accurately quantified surface PM<sub>2.5</sub> concentrations and AOD simultaneously and at a substantially lower cost and smaller size than existing equipment. To test implementation of the AMODv1, we constructed and deployed 25 AMODv1s in a citizen-science network, as documented in part 2 in this series (Ford et al., 2019).

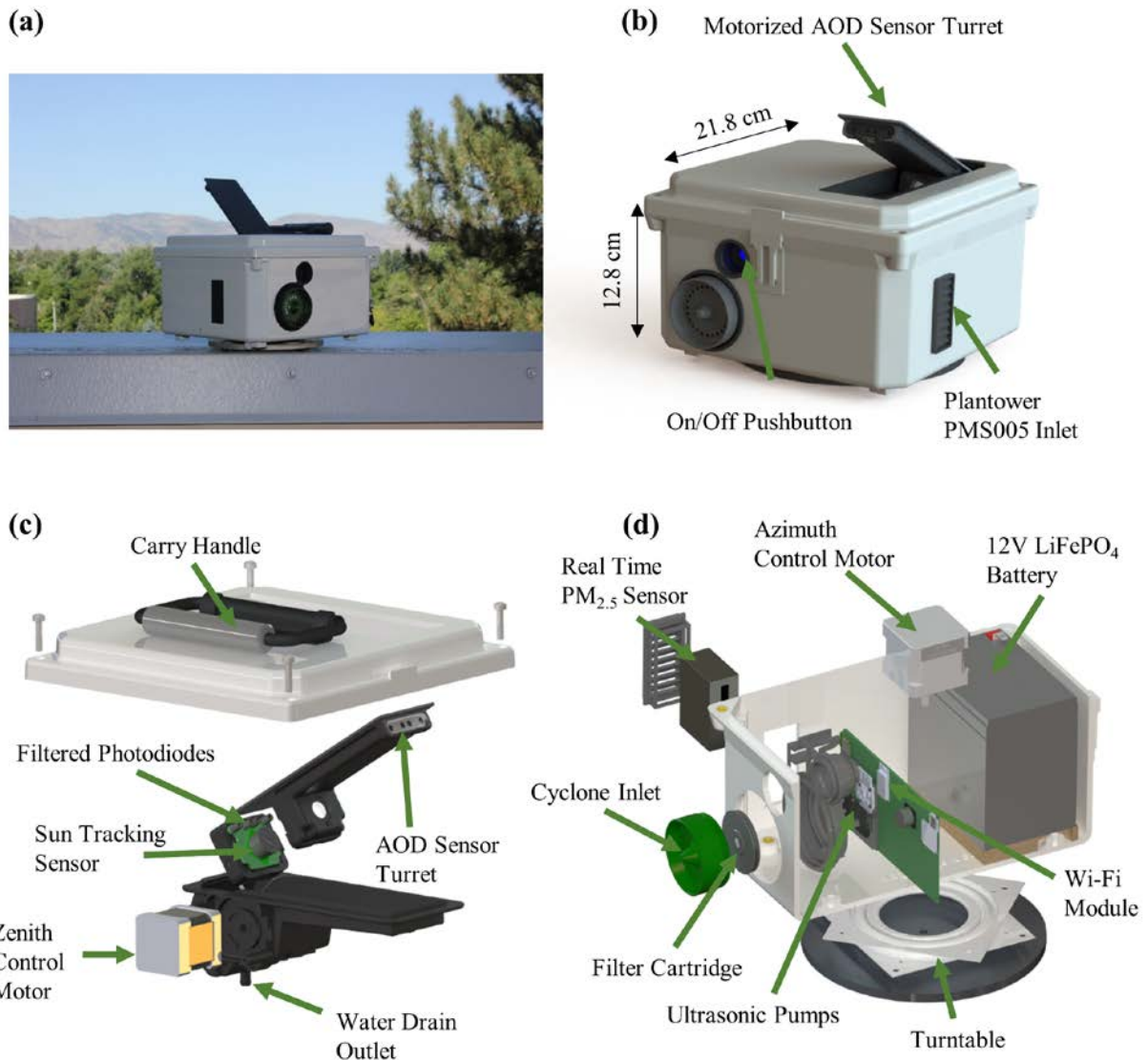
Despite the promise of the AMODv1, the initial deployment highlighted several key limitations. First, the AMODv1 lacked quality control measures for misalignment or cloud contamination during the measurement period. Second, the instrument had limited temporal resolution for AOD (typically one measurement per day). Third, despite the presence of a visual alignment aid (Wendt et al., 2019), many volunteers found it difficult to align the instrument with the sun, which was compounded by inconsistent standards as to what constituted proper alignment. Fourth, data could not be transmitted wirelessly or accessed remotely. The first objective of this current work was to address these four major limitations of the AMODv1 design. Another shortcoming of our work on AMODv1 was limited stability analysis of the AOD sensors across varying atmospheric conditions and over time. The second objective of this work, therefore, was to evaluate the stability of the AOD sensors across a range of pollution levels and to assess the stability of the AOD sensors after repeated deployments over the course of a year. Here, we describe our design changes and extended validation efforts toward our research objectives. First, we summarize the design advantages of the AMODv2 relative to the AMODv1. Second, we present the results from a validation campaign where AMODv2 units were co-located with reference instruments. Third, we analyse the stability of AMODv2 AOD measurements after 15 months of use. Finally, we analyse the reliability of the AMODv2 design in a series of laboratory experiments. The results presented here demonstrate that AMODv2 is a practical option to establish spatially-dense PM<sub>2.5</sub> and AOD measurement networks. Applied in these networks, the AMODv2 will

close gaps in the existing global aerosol measurement infrastructure of ground-based and satellite-based observations.

## 145 **2 Materials and methods**

### **2.1 Instrument design**

We designed the AMODv2 to sample integrated gravimetric  $PM_{2.5}$  mass concentration, real-time  $PM_{2.5}$  mass concentration, and AOD simultaneously. One intended application is large-scale sampling campaigns with the AMODv2 instruments operated by volunteers with little to no background in aerosol or atmospheric science (Ford et al., 2019). Thus, we prioritized a design that is low-cost, accurate, mechanically robust, portable, automated, and user-friendly. We provide images of AMODv2 hardware in Fig. 1, highlighting key internal and external components.



155 **Figure 1: Images detailing external and internal AMODv2 design and hardware. a) Photograph of AMODv2 sampling outdoors. b) External computer animated rendering of AMODv2 features and dimensions. c) Computer generated exploded view of AOD measurement subsystem. d) Computer generated exploded section view of PM<sub>2.5</sub> sampling, wireless data transfer, and power subsystems.**

160 The AMODv2 measures AOD at 440 nm, 500 nm, 675 nm, and 870 nm using optically filtered photodiodes (Intor Inc., Socorro, NM, USA) with narrow bandwidth (<15 nm at full-width half-maximum signal). The measurement process is fully automated using a solar tracking system (Section 2.3), reducing the potential for misalignment due to user error. Movement in the zenithal plane is achieved using a custom turret module embedded in the interior of the AMODv2 enclosure (Fig. 1a). The module was designed in SolidWorks® (ANSYS, Inc.,

165 Canonsburg, PA, USA) and built using multi-jet fusion printing. The module houses a custom printed circuit board containing the solar tracking sensors and the filtered photodiodes. Light enters the turret through four, 4 mm

apertures, and passes through 112 mm tubes to reach the filtered photodiodes (Fig. 1c). These proportions yield a viewing angle of approximately 2 degrees for each photodiode sensor element. A stepper motor (Stepper Online 17HS10-0704S-C2, Nanjing City, China), fixed to the turret, actuated the zenithal rotation. Movement in the azimuthal plane is actuated using a second stepper motor (Stepper Online 17HS19-1684S-C6, Nanjing City, China) fixed to a turntable and base-plate assembly (McMaster Carr 6031K16, Elmhurst, IL, USA), which enables 360 degree rotation of the AMODv2. The angular resolution of each stepper motor is tuned to 0.056 degrees using programmable drivers (Texas Instruments DRV8834RGER, Dallas, Texas, USA). Active tracking is accomplished using closed-loop control enabled by a 3-axis accelerometer (STMicroelectronics LSM6DSM, Geneva, Switzerland), a GPS module (u-blox CAM-M8, Thalwil, Switzerland), and a quadrant photodiode solar tracking sensor (Solar MEMS NANO-ISS5, Seville, Spain).

The AMODv2 measures  $PM_{2.5}$  using both real-time and time-integrated techniques. Real-time  $PM_{2.5}$  concentrations are measured and streamed using a light-scattering  $PM_{2.5}$  sensor (Plantower PMS5003, Beijing, China). A 3D-printed fixture secured the sensor in position to sample ambient air, while downward sloping vents protect the sensor from water ingress (Fig. 1d).  $PM_{2.5}$  concentrations are evaluated on the PMS5003 chip via a manufacturer proprietary algorithm. The AMODv2 reports the  $PM_{2.5}$  values corrected by Plantower's proprietary atmospheric correction. These values are accessed by the AMODv2 microcontroller via serial communication. A flow chart detailing the  $PM_{2.5}$  measurement protocol is provided in Fig. S1.

For time-integrated  $PM_{2.5}$  mass concentration measurement, we leveraged a  $PM_{2.5}$  cyclone design from prior studies (Volckens et al., 2017; Kelleher et al., 2018; Wendt et al., 2019). The main circuit board features three ultrasonic pumps (Murata MZBD001, Nagaokakyo, Japan) and a mass flow sensor (Honeywell Omron D6F, Charlotte, NC, USA,) to control the flow of air through a custom aluminum cyclone and filter cartridge with a 50% cut point of 2.5  $\mu m$  (Fig. 1d). The gravimetric sample is collected on a 37mm Teflon filter secured within a filter cartridge. Sampled particles are collected on a single filter that is pre and post weighed for each sample. During deployment, a field blank is carried along with the sampler to correct for incidental mass contamination or drift.

The AMODv2 is powered using a 12 V, 10 Ah  $LiFePO_4$  battery (Dakota Lithium, Grand Fork, ND, USA) with a secondary 12 V, 3.3Ah  $LiFePO_4$  (Battery Space, LFH4S4R1WR-C5, Richmond, CA, USA) battery in parallel. The battery is charged using a barrel plug inlet accessible on the side of the enclosure. A detachable rubber plug seals the inlet from the outside environment when not charging. Charging circuitry supports charging at a rate of 3.0 A, enabling a full charge in approximately eight hours. A full charge can power the AMODv2 for over 120 hours.

The AMODv2 records and wirelessly transfers meteorological and quality-control data in real time. Meteorological data include ambient temperature ( $^{\circ}C$ ), ambient pressure (hPa), and relative humidity (%). Quality control metrics include sample duration (s), sample flow rate ( $L\ min^{-1}$ ), total sampled volume (L), battery temperature ( $^{\circ}C$ ), battery voltage (V), battery state of charge (%), current draw (mA), and wireless signal strength (RSSI).

The external housing of the AMODv2 (Fig. 1b) is made from a weather-resistant NEMA electrical enclosure (Polycase, YQ-080804, Avon, Ohio, USA). The dimensions of a fully assembled AMODv2 are 21.8 cm

W × 21.8 cm L × 12.8 cm H, with a weight of 3.1 kg. A folding carry handle is fixed to the upper surface of the enclosure to aid transport (Fig. 2b). The total cost of the AMODv2 was \$1,175 per unit, for a production run of 100 units (Table S1). This tabulation includes an estimated three hours of assembly at a rate of \$25 per hour.

We developed the AMODv2 control software using an online, open-source platform (mbed™; ARM® Ltd., Cambridge, UK). The software was written in C++ and executed by a 64-bit microcontroller (STMicroelectronics STM32L476RG, Geneva, Switzerland). We implemented wireless data transfer using a Wi-Fi and Bluetooth™ module (Espressif Systems ESP32-C3-WROOM, Shanghai, China). A MicroSD card stores all data for data backup or offline deployment (Molex 5031821852, Lisle, IL, USA). We integrated software modules for AOD, real-time PM<sub>2.5</sub>, gravimetric PM<sub>2.5</sub>, data logging, and wireless data transfer using a real-time operating system (RTOS) for pseudo-simultaneous software execution.

## 2.2 AOD measurement and solar tracking

The AMODv2 applies the Beer-Lambert-Bouguer law to calculate AOD ( $\tau_a$ ). This relationship, expressed in terms of measurable parameters, is as follows:

$$\tau_a(\lambda) = \frac{1}{m} \left( \ln \left( \frac{V_0}{R^2} \right) - \ln(V) \right) - \tau_R(\lambda, p) - \tau_{O_3} \quad (2)$$

where  $m$  is the unitless air mass factor, which accounts for the increased air mass that light passes through as the sun approaches the horizon,  $R$  is the Earth-sun distance in astronomical units (AU),  $V$  is the signal produced by the light detector in volt,  $\tau_R$  accounts for Rayleigh scattering by air molecules,  $p$  is the pressure at the sensor in Pa,  $\lambda$  is the sensor wavelength in m,  $\tau_{O_3}$  accounts for ozone absorption, and  $V_0$  is the extraterrestrial constant in volts, which is the sensor signal if measured at top-of-atmosphere and is determined via calibration. AOD values at 440 nm, 500 nm, 675 nm, and 870 nm are calculated using Eq. (2). The Earth-Sun distance,  $R$ , is computed directly from GPS data and the solar positioning algorithm.  $V$  is the signal produced by the photodiode and  $V_0$  is accessed from on-chip memory. The relative optical air mass factor is computed as a function of solar zenith angle ( $\theta$ ) as follows (Young, 1994):

$$m = \frac{1.002432 \cdot \cos^2(\theta) + 0.148386 \cdot \cos(\theta) + 0.0096467}{\cos^2(\theta) + 0.149864 \cdot \cos^2(\theta) + 0.0102963 \cdot \cos(\theta) + 0.000303978} \quad (3)$$

The contribution of total optical depth from Rayleigh scattering,  $\tau_R$ , is calculated based on wavelength and ambient pressure measured by an ambient pressure sensor mounted on the circuit board with the AOD sensors (Bosch Sensortec BMP 280, Kusterdingen, Germany) (Bodhaine et al., 1999). Ozone concentration is estimated using an empirical model based on time of year and location, and converted to  $\tau_{O_3}$  using wavelength-specific ozone absorption coefficients (Griggs, 1968; Van Heuklon, 1979). With all parameters known, Eq. (2) is applied to calculate AOD.

We implemented automatic solar tracking capabilities using a suite of low cost sensors and a multi-stage algorithm. Detailed flow charts of the AOD measurement protocol are provided in the supplementary Figs. S2-S6. The open-loop stage is initiated when the microcontroller requests an AOD measurement and the GPS time and location is computed. Using this information, the AMODv2 applies a solar positioning algorithm from the National Renewable Energy Laboratory (NREL) to compute the solar elevation angle (Reda and Andreas, 2008). The

calculated solar zenith angle is then compared with the pitch of the AOD turret relative to horizontal. The turret  
240 stepper motor rotates the turret in the direction of the sun until the elevation angle of the AOD turret is  
approximately equal to that of the sun. The base motor rotates counterclockwise in order to achieve approximate  
azimuth alignment. After every 10 degrees of azimuthal rotation, the total signal of the sun-tracking quadrant  
photodiode is compared with an empirical threshold. If the threshold is exceeded, the AMODv2 enters closed-loop  
tracking. If the threshold is not exceeded on the first revolution, the AMODv2 executes a second revolution before  
245 ending the search protocol.

In the closed-loop tracking stage, the rotation of the motors is controlled using the zenithal and azimuthal  
error signals produced by the quadrant photodiode. The quadrant photodiode is mounted in a diamond orientation,  
with two quadrants forming a vertical axis, and two forming a horizontal axis. The vertical error signal is the ratio of  
the top and bottom quadrants and the horizontal error signal is the ratio of the right and left quadrants. The stepper  
250 motors rotate independently until each error signal is reduced within an experimentally determined threshold. The  
motors then lock in place while an AOD measurement is recorded. The AMODv2 measures AOD as triplet sets.  
Between each measurement, both motors disengage for 30 seconds to conserve power. After 30 seconds, the  
AMODv2 executes the tracking algorithm and records an AOD measurement. This process is repeated until the  
triplet set is completed or until 3 minutes have elapsed since the initial measurement request was made by the  
255 processor.

Real-time quality control is performed on each measurement triplet. Empty or incomplete triplets are  
flagged and assigned an error code. Completed triplets are screened for cloud contamination using the AERONET  
triplet cloud screening algorithm (Smirnov et al., 2000; Giles et al., 2019). The algorithm takes the maximum  
deviation of any two measurements within a triplet, and applies thresholds to mark triplets as clear or cloud-  
260 contaminated (Smirnov et al., 2000; Giles et al., 2019). Large deviations of AOD within a triplet are more likely due  
to cloud contamination than changes in aerosol loading (Smirnov et al., 2000; Giles et al., 2019). Measurements  
identified as cloud-contaminated are flagged with a unique numerical code. Measurements with incomplete triplets  
are also flagged with a unique numerical code.

### 2.3 AOD calibration procedure

The extraterrestrial constants for all AMODv2s were evaluated via calibration relative to AERONET sun  
photometers (Cimel CE318, Paris, France) (Holben et al., 1998). AERONET instruments report AOD at 340 nm,  
380 nm, 440 nm, 500 nm, 675 nm, 870 nm, 1020 nm, and 1640 nm (Holben et al., 1998). We selected the four  
AMODv2 AOD wavelengths in part for direct comparison with AERONET instruments. We conducted calibrations  
at the MAXAR-FUTON site in Fort Lupton, Colorado (40.036 N, 104.885 W) between November 2019 and  
270 February 2020. AMODv2 units were co-located within 50 m of the AERONET instrument and sampled for 2 to 3  
hours at a rate of one sample every 2.5 to 3 minutes (note: AERONET instruments are programmed to record AOD  
every 15 min so we oversampled the AMODv2 to achieve sufficient temporal overlap with AERONET). AMODv2  
and AERONET level 1.0 measurements concurrent within 60 seconds of each other were included in the calibration  
data set (Holben et al., 1998). For each set of concurrent measurements, we calculated the extraterrestrial constant

275 by applying Eq. (2) solved for  $V_0$ , where  $V$  was the raw voltage reported by the AMODv2, and  $\tau_a$  was the AOD reported by the AERONET instrument. The AMODv2 calibration constants were the average value of  $V_0$  for a given instrument and wavelength.

#### **2.4 User operation and measurement procedure**

280 We designed the AMODv2 to be operated by individuals without a background in aerosol sampling. We developed a standard procedure that is detailed in a user manual provided as supplementary material. After the initial setup, the AMODv2 requires no operator inputs for the duration of the sample. A flow chart outlining the manual and automatic steps to perform an AMODv2 measurement is provided in Fig. 2.

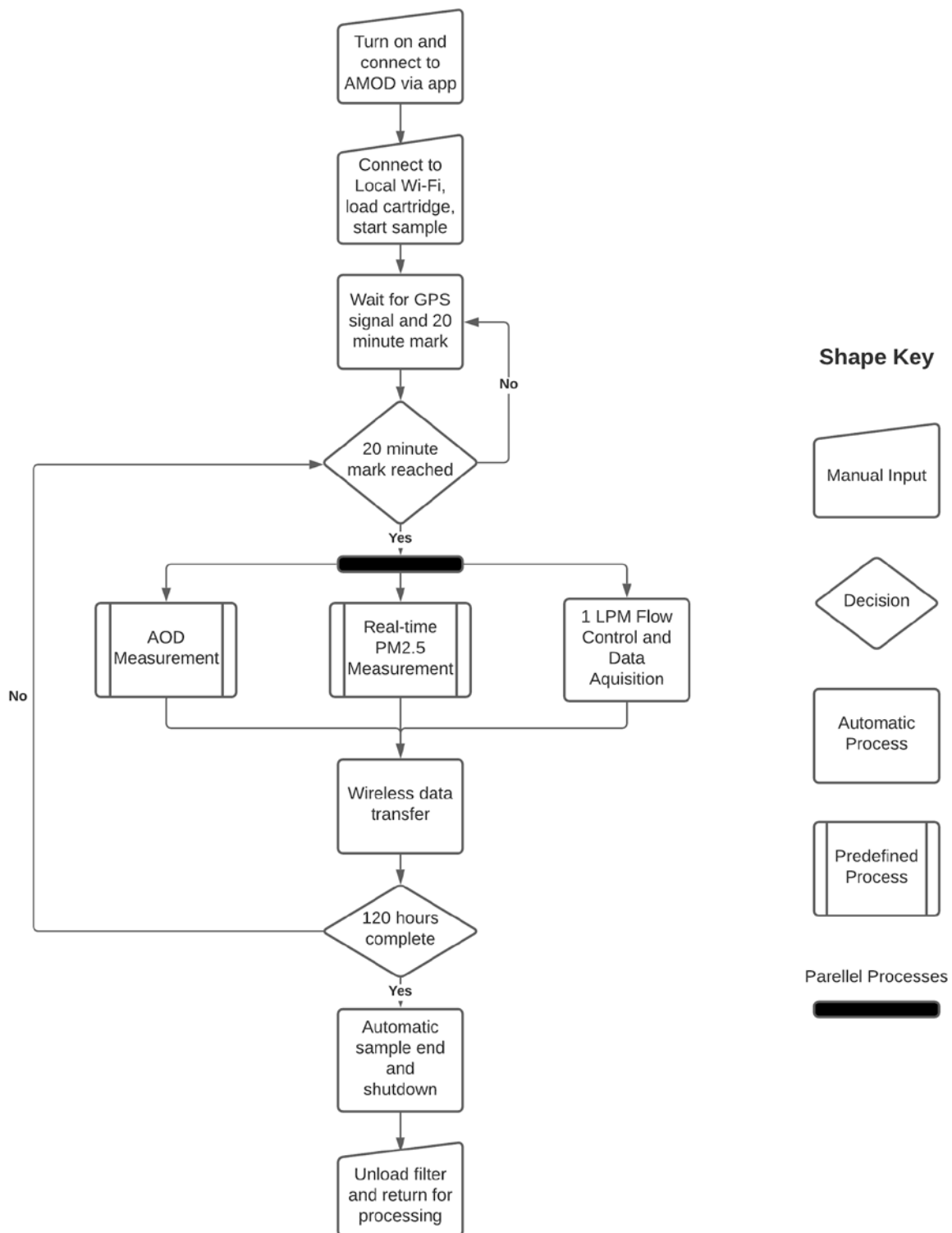


Figure 2: Overall device operation flow diagram for a single sample. After each sample, the AMODv2 must be recharged for at least eight hours. Manual inputs require operator intervention. Automatic processes are executed with no operator

**intervention. Predefined processes are detailed in supplemental Figs. S1-S6. Parallel processes are executed pseudo-simultaneously using a real-time operating system.**

290 Materials needed to initiate a sample include an AMODv2, a cartridge loaded with a pre-weighed filter, and  
a smartphone with the AMODv2 control application installed (“CEAMS”; available on the Apple App Store and  
Google Play) (Quinn 2019). A detailed description of the mobile application is in the user manual, which is included  
as a supplement to this work. After executing an initialization routine by selecting “Scan for Device”, the operator  
may connect to their device via Bluetooth™ using the mobile application. The operator can select a wireless  
network and input the proper credentials to connect the AMODv2 to the internet. The application then prompts the  
operator to scan the QR code on the back of the filter cartridge to link the filter with the upcoming sample in the data  
log. After the cartridge is manually loaded into the compartment behind the inlet (Fig. 1b), the AMODv2 should be  
placed on a flat surface with an unobstructed view of the sun. The operator then starts the sample from the mobile  
application. After an initial data push, the sample begins at the next 20 minute mark (e.g. 12:00, 12:20, or 12:40).  
The AMODv2 begins sampling air through the inlet at 1 L min<sup>-1</sup> and continues to do so for the remainder of the 120-  
hour sampling period. Real-time PM<sub>2.5</sub> and AOD measurements are initiated at each 20 minute mark from the start  
of the sample. The PM<sub>2.5</sub> reported at each 20 minute interval is the average of measurements taken every 10 seconds  
over a period of 3 minutes. If the sun is less than 10 degrees above the horizon, the motors do not activate and the  
solar tracking algorithm is not executed. After each AOD and PM<sub>2.5</sub> measurement is completed, data are uploaded to  
the affiliated website (csu-ceams.com), where real-time visualizations of AOD and PM<sub>2.5</sub> are available. Data  
reported to the website are accessible with a map-based user interface. Quality-control data are available to research  
staff via a private administrator portal. A snapshot example of the website is provided in Fig. S7. At the conclusion  
of a sample, the operator removes the filter cartridge. Upon receipt of the filters, the CEAMS team stored the filters  
in the refrigerator until mailed to minimize loss of volatile compounds. Complete data files can be downloaded from  
the website or accessed via a MicroSD card. Individual measurements of AOD and PM<sub>2.5</sub>, from which averages are  
derived, are available in the complete file, facilitating post-sample uncertainty analysis of PM<sub>2.5</sub> and AOD  
measurements.

## 2.5 Validation, stability, and reliability studies

315 We assessed precision and bias of AMODv2 AOD sensors relative to an AERONET monitor at the NEON-  
CVALLA site in Longmont, Colorado (40.160 N, 105.167 W) between June 2020 and December 2020 (Holben et  
al., 1998). We co-located our instruments within 50 m of the reference instrument (and within 5 m of each other) on  
nine separate days with varying atmospheric conditions (e.g. wildfire smoke and clean air) using a total of 14 unique  
AMODv2 units. Each test consisted of 2 to 4 hours of sampling at a rate of one sample approximately every 3  
minutes. The AERONET reference monitor sampled at a frequency of one sample approximately every 15 minutes.  
AMODv2 and AERONET measurements concurrent within 2 minutes were included in the validation data set. The  
accuracy of AMODv2 AOD measurements was assessed via Deming regression.

We evaluated the long-term stability of the AOD sensors by re-calibrating a set of 16 AMODv2 units 15 months after their initial calibration. Original calibrations for the units tested were conducted at the MAXAR-FUTON site in Fort Lupton, Colorado, USA (40.036 N, 104.885 W) on February 21, 2020. Re-calibrations were conducted at the NEON-CVALLA site on May 27, 2021 (The MAXAR-FUTON site was indefinitely unoperational at the time of the second calibration).

We tested the reliability of AMODv2 instruments in a series of 5-day, outdoor samples on the roof of a Colorado State University laboratory facility (430 N College Avenue, Fort Collins, Colorado, USA). All units were co-located within a 10 m radius. We started tests on January 16, 2021, January 30, 2021, and March 31, 2021, which included 34, 27, and 15 unique AMODv2 units respectively, for a total of 76 samples. We assessed the reliability of the AMOD according to the rate at which samples terminated prematurely. Samples that failed to reach at least 115 hours of the intended 120 hour sample duration were designated as premature terminations. We specifically assessed the mechanical robustness of AMODv2 units by visually inspecting failed units for evidence of water ingress and electrical component damage. We also analyzed the AOD data from these samples to evaluate the automatic solar alignment procedure and quality control algorithm.

Compared with our prior work (Wendt et al., 2019), we tested the AMODv2 AOD measurement system under a broader range of atmospheric conditions. A sizable portion of validation measurements were taken under heavy smoke caused by the Cameron Peak and East Troublesome fires of 2020. We conducted additional testing under more moderate smoke and clear conditions. AOD values reported by AERONET during validation experiments ranged from  $0.035 \pm 0.01$  to  $1.59 \pm 0.01$  at 440 nm,  $0.030 \pm 0.01$  to  $1.51 \pm 0.01$  at 500 nm,  $0.021 \pm 0.01$  to  $1.130 \pm 0.01$  at 675 nm, and  $0.016 \pm 0.01$  to  $0.770 \pm 0.01$  at 870 nm.

### 3 Results and discussion

#### 3.1 Summary of design improvements

With the AMODv2 design presented here, we addressed the key shortcomings that we identified with AMODv1 enumerated in the Introduction. First, AOD quality control was addressed with motorized solar tracking and a cloud screening protocol. AMODv2 AOD measurements are taken as triplets, facilitating the application of screening protocols based on temporal variation (Smirnov et al., 2000; Giles et al., 2019). The availability of full data files at the end of each sample facilitates additional screening based on hourly and daily variations in AOD values, beyond the immediate quality controls applied to triplets. Second, insufficient temporal resolution was addressed by automating AOD measurement and increasing the sample rate. With automatic sampling in place, units measure every 20 minutes of daylight for up to five days. This updated protocol increases the likelihood that measurements will be available at the desired times of day (e.g. satellite overpass times). Third, we reduced the potential for operator error by eliminating the manual alignment requirement present in the prior design via solar tracking. Fourth, we improved data accessibility through the integration of a Wi-Fi module and a user-friendly website interface. These design changes were achieved while adding only \$75 to the manufacturing cost, relative to AMODv1 (Table S2). The most important design changes from AMODv1 to AMODv2 are summarized in Table 1.

**Table 1: Design comparison between AMODv1 and AMODv2**

Design specification	AMODv1	AMODv2
Sample interval	48 hours	120 hours
Sample flow rate	2 L min <sup>-1</sup>	1 L min <sup>-1</sup>
Sun alignment procedure	Manual using pinhole aperture target	Automatic dual-axis closed-loop sun tracking system
AOD cloud screening	None available	Automatic AOD triplet measurement screening protocol
AOD measurement frequency	1 measurement per day	1 measurement every 20 minutes during daytime hours
Data logging	MicroSD card	MicroSD card, wireless data transfers every 20 minutes, and complete file wireless data transfer at the end of each sample
Data visualization	None available	Real-time PM <sub>2.5</sub> and AOD plots on website
Real-time debugging information	None available	Sample flow rate, total sampled volume, battery temperature, battery voltage, state of charge, current draw, and wireless signal strength
Manufacturing Cost (As of July 2019)	\$1,100	\$1,175

We conducted a sample deployment of 10 AMOD units during a wildfire smoke event in Fort Collins, Colorado in October of 2020. The purpose of this deployment was to highlight the design advantages of the AMODv2 in the context of rapidly changing air quality. The results of the deployment are detailed in the first supplement to this work (Figs. S8 and S9).

### 3.2 AOD sensor validation and calibration stability

Here, we present results of co-located validation studies for the AOD measurement system. Our cyclone-based gravimetric PM<sub>2.5</sub> sampling system has been validated extensively in prior work and shown to agree closely with reference PM<sub>2.5</sub> monitors (Volckens et al., 2017; Arku et al., 2018; Kelleher et al., 2018; Pillarisetti et al., 2019; Wendt et al., 2019). Plantower light scattering sensors have likewise been evaluated extensively in prior work (Kelly et al., 2017; Zheng et al., 2018; Levy Zamora et al., 2019; Sayahi et al., 2019; Wendt et al., 2019; Bulot et al., 2019; Tryner et al., 2020).

370 We observed close AOD agreement between AMODv2 and AERONET instruments. Correlation plots on  
 the full set of measurement pairs are provided in Fig. 3 (n = 426 paired measurements per wavelength). Summary  
 statistics calculated on the full set of measurement pairs across all measurement conditions are provided for each  
 wavelength in Table 2.

375 **Table 2: Summary statistics for AMODv2 vs. AERONET co-located tests**

Wavelength (nm)	Mean absolute error (AOD)	Deming slope coefficient	R <sup>2</sup>	AOD Precision (AOD)
440	0.04	0.953	0.987	0.02
500	0.06	0.985	0.978	0.03
675	0.03	1.011	0.995	0.01
870	0.03	1.015	0.977	0.02

Summary statistics on the data set partitioned into clear and elevated-AOD samples are presented in Table S1. The definitions of clear and elevated-AOD samples are explained in the description of Table S1. The mean absolute errors for the full data set were 0.04, 0.06, 0.03, and 0.03 AOD units at 440 nm, 500 nm, 675 nm, and 870 nm, respectively. The Deming regression slope coefficients were 0.953, 0.985, 1.011 and 1.015 at 440 nm, 500 nm, 675 nm, and 870 nm, respectively. The squares of Pearson correlation coefficients were 0.987, 0.978, 0.995, and 0.977 at 440 nm, 500 nm, 675 nm, and 870 nm, respectively. With respect to precision, the average differences from the mean for units measuring coincidentally (i.e. the average amount an individual unit deviated from the mean of all units measuring at the same time) were 0.02, 0.03, 0.01, and 0.02 AOD units at 440 nm, 500 nm, 675 nm, and 870 nm, respectively. With respect to stability across AOD magnitude, the mean absolute error deviated by less than 0.011 between clear days and elevated-AOD days across all wavelengths (Table S1).

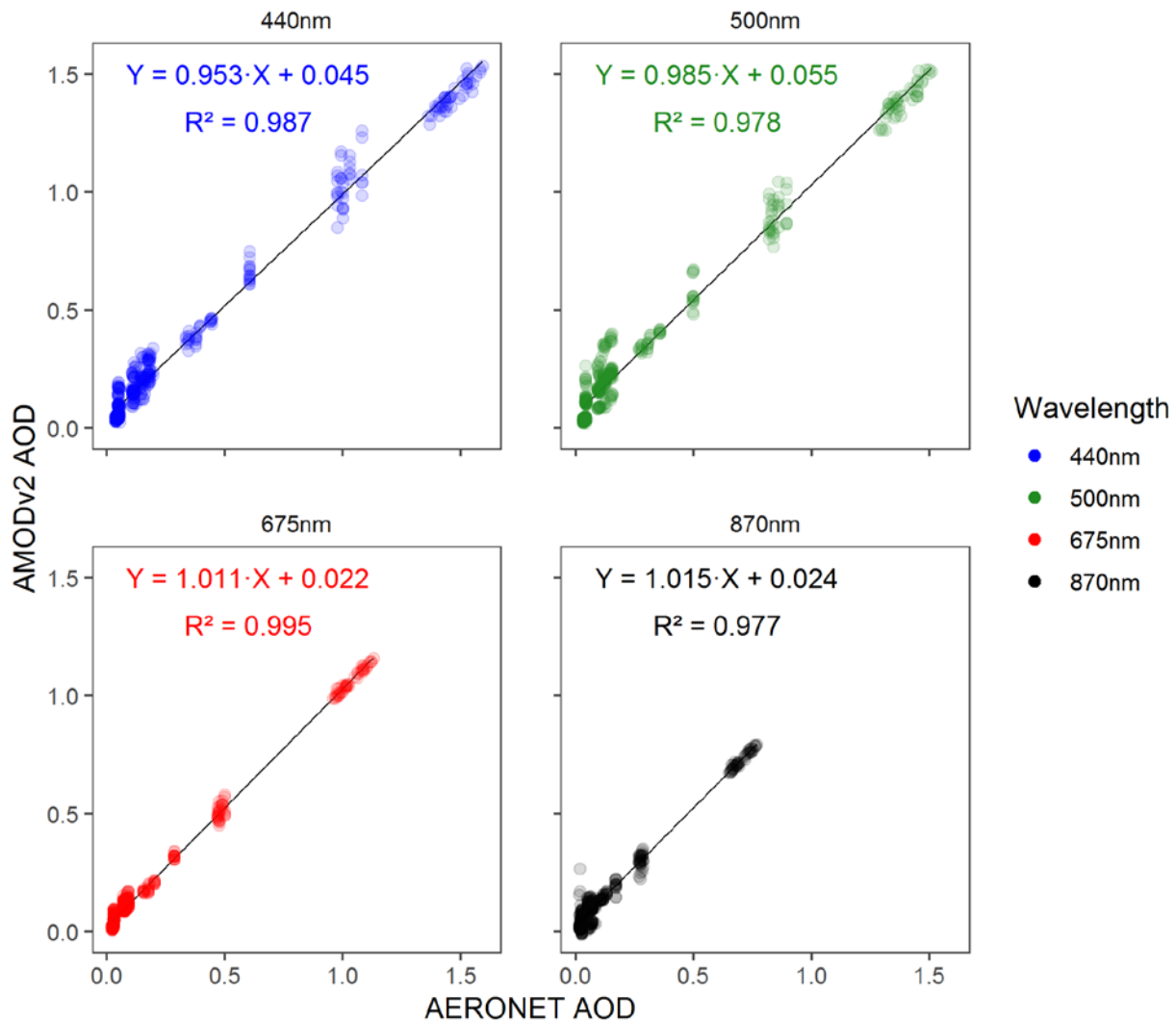


**Figure 3: AERONET (MAXAR-FUTON site in Fort Lupton, Colorado, USA) vs. AMODv2 AOD co-located comparison (n=426) results with panels separated by wavelength. Lines of best fit were calculated via deming regression analysis.**

390

Due to the broad range of AOD levels during testing, global summary statistics do not fully capture how error and precision scales with increasing AERONET AOD, as these figures of merit are not constant across the range of measured AOD values (Fig. 4). Measurements at high AOD impact the mean absolute error disproportionately, while measurements at low AOD impact the mean percent error disproportionately. We derived expected error (EE) equations to constrain the error of AMODv2 measurements relative to AERONET as a function of AOD (following the form used in the validation of satellite AOD products compared to AERONET AOD). We

395

derived the equations iteratively by adjusting the constant and linear terms until the bounds defined by Eqs. (4) through (7) each contained 85% of the co-located measurement pairs for each wavelength.

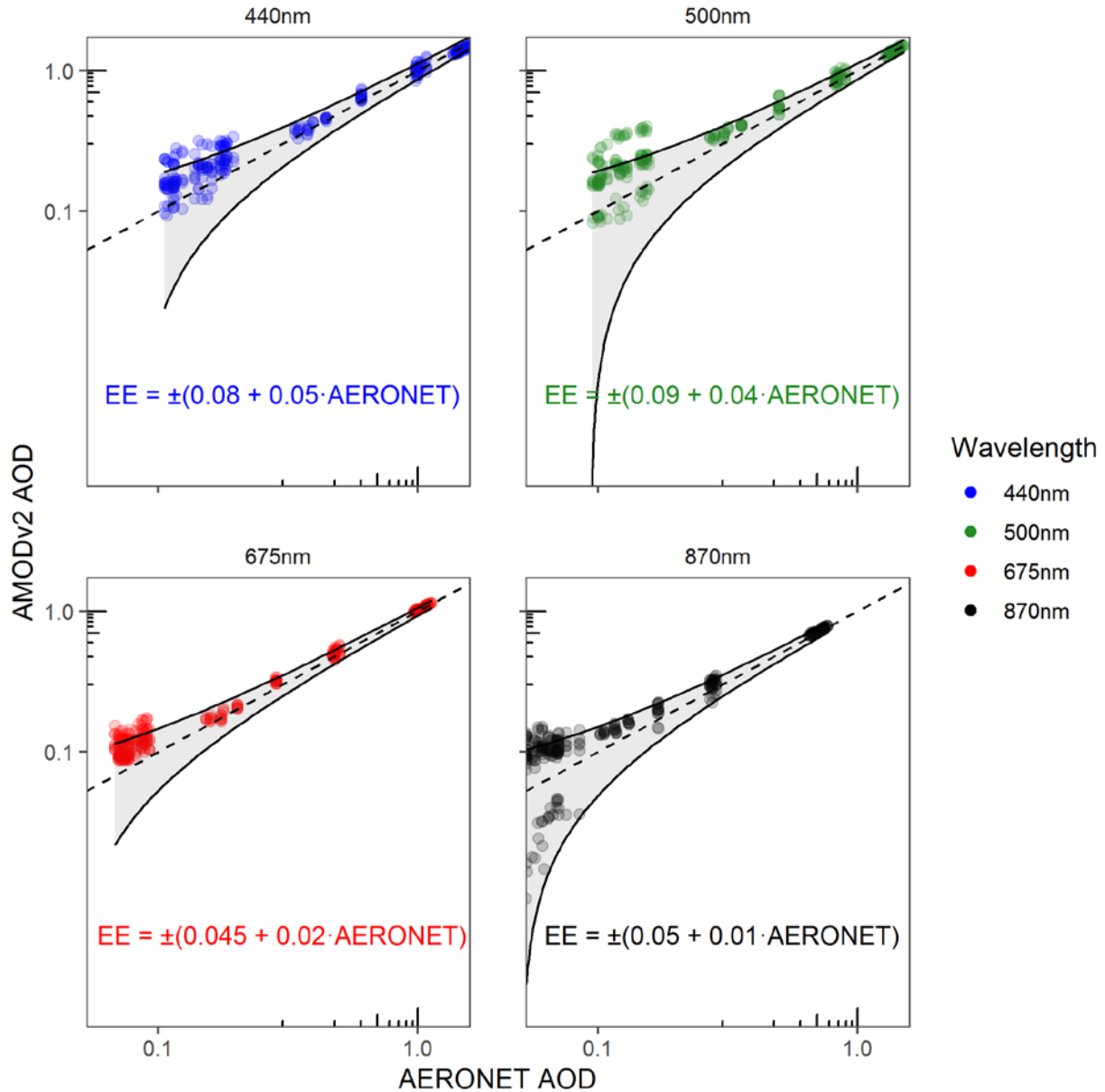
$$EE_{440} = \pm(0.080 + 0.050 \cdot AOD_{AERONET440}) \quad (4)$$

$$400 \quad EE_{500} = \pm(0.090 + 0.040 \cdot AOD_{AERONET500}) \quad (5)$$

$$EE_{675} = \pm(0.045 + 0.020 \cdot AOD_{AERONET675}) \quad (6)$$

$$EE_{870} = \pm(0.050 + 0.010 \cdot AOD_{AERONET870}) \quad (7)$$

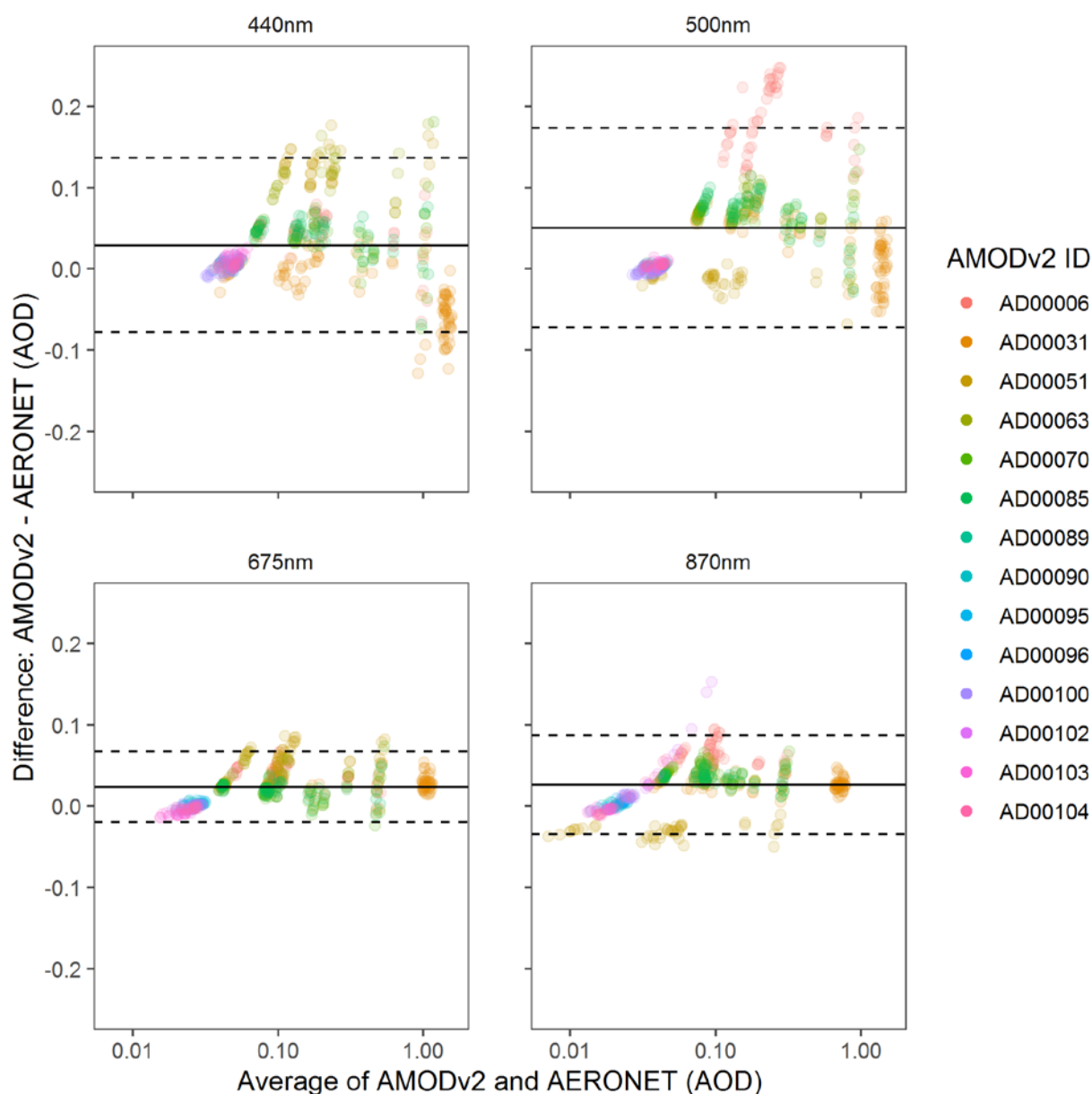
A logarithmic plot illustrating how the error bounds scale with increasing AOD is provided in Fig. 4.



405 **Figure 4: Logarithmic AERONET vs. AMODv2 AOD co-located results with expected error (EE; AOD units) bounds, with panels separated by wavelength. Equation bounds contain 85% of co-located measurements.**

Equations (4) through (7) indicate a low dependence of the AOD magnitude on the AMODv2 error relative to AERONET for all wavelengths. Existing error between AMODv2 and AERONET measurements was explained primarily by the constant term. These findings are consistent with the summary statistics presented in Table S1 and demonstrate the stability of AMODv2 .

AMODv2 bias relative to AERONET was primarily dependent on the specific unit, rather than systemic design uncertainty. A mean-difference plot colored by AMODv2 unit ID is provided in Fig. 5.



415 **Figure 5: Mean-difference plot for measurements taken by AERONET and AMODv2 instruments, with panels separated by wavelength. Paired AERONET and AMODv2 under both clear and biomass burning conditions (as defined in Table S1) are included. Points represent paired AMODv2 and AERONET measurements with the average of the measurement pair on the x-axis in log scale and the difference on the y-axis. The top and bottom dashed lines represent the upper and**

420 **lower limits of agreement, respectively, evaluated at 95% confidence. The solid line in between the limits of agreement is**  
**the mean difference between the two measurement techniques. Points are colored according to the AMODv2 unit ID.**

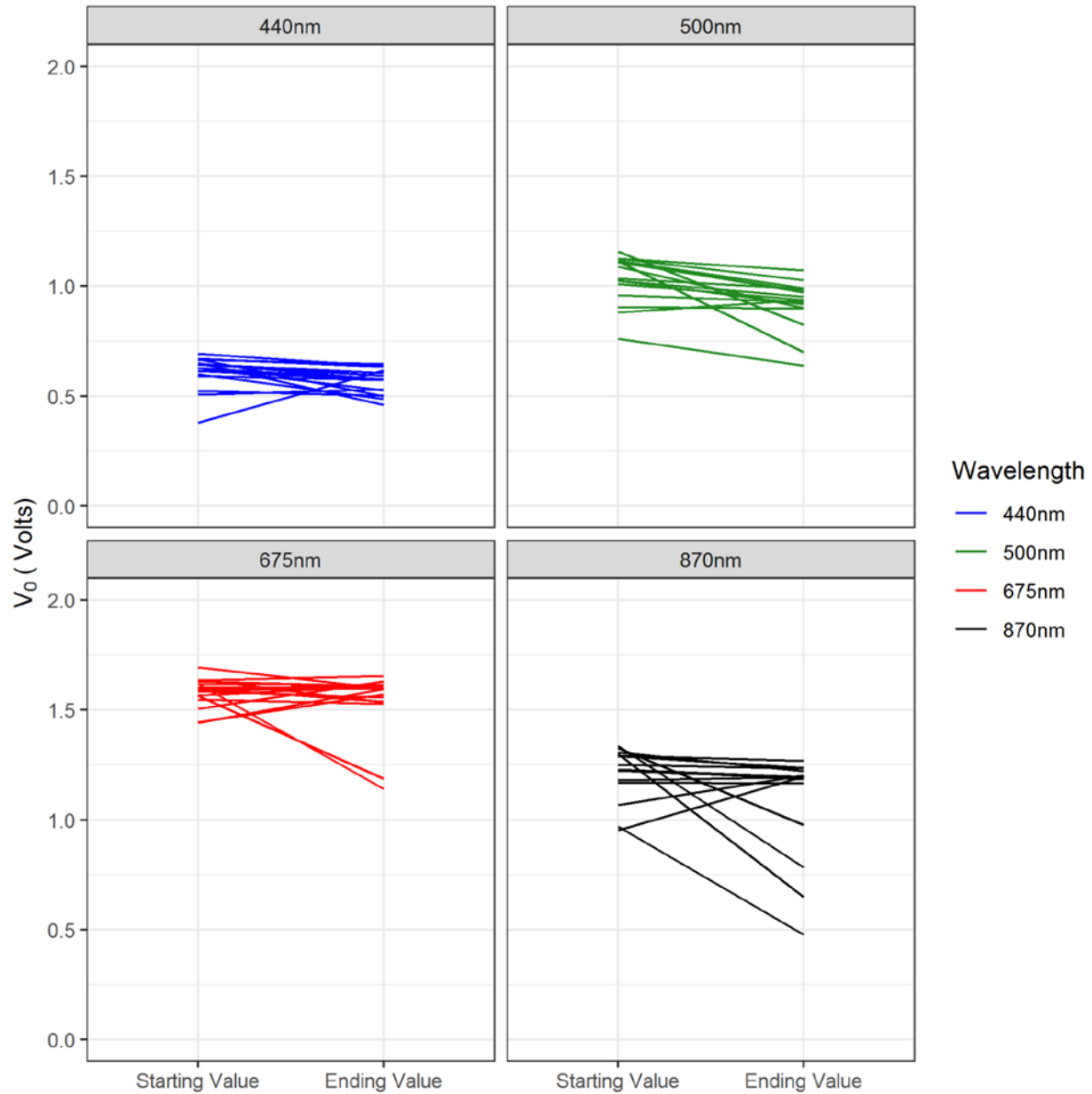
425 Units AD00006 and AD00051 exhibited the highest bias at 440 nm and 500 nm, respectively. With units  
 AD00051 and AD00006 removed from the data set, mean absolute errors were reduced by 0.011, 0.013, 0.008, and  
 0.004 AOD units at 440 nm, 500 nm, 675 nm, and 870 nm, respectively. Bias from units AD00006 and AD00051  
 430 also impacted the EE derivations. With units AD00006 and AD00051 omitted, Eqs. (4) through (7) bound 92.5%,  
 94.6%, 97.6% and 92.2% of the co-located pairs, respectively. Individual unit bias was most likely caused by faulty  
 calibration or optical sensor drift over time.

430 Previous work has noted the tendency for optical interference filters to degrade over time, changing the  
 accuracy of the most recent calibration (Brooks and Mims, 2001; Giles et al., 2019). We quantified the long-term  
 stability of the AMODv2 AOD sensors by re-calibrating 16 AMODv2 units 15 months after their initial calibration.  
 Summary statistics quantifying the change calibration constant ( $V_0$ ) changes are provided in Table 3.

**Table 3: Summary statistics for AMODv2 calibration stability test. All summary statistics refer to the change in  $V_0$  (Eq. 2). Note that the absolute value of the maximum change refers to the single unit with the highest percent change for each wavelength.**

Wavelength (nm)	Average absolute value of change (%)	Median change (%)	Absolute value of maximum change (%)
440	13.84	-7.14	62.72
500	11.80	-9.64	37.08
675	6.66	-0.75	29.40
870	14.63	-2.80	50.72

435 A plot illustrating the voltage change undergone by each of the 16 AMODv2 units is provided in Fig. 6.



440 **Figure 6: Linear change plots illustrating the change in calibration voltage,  $V_0$  (Eq. 2), from the initial calibration to a follow up test calibration of 16 AMODv2 units. Each instrument is represented by a separate line with starting and ending calibration voltage values delineated on the vertical axis. Panels are separated by wavelength. Each line represents the change after 15 months of a single wavelength channel of an AMODv2 unit.**

The results presented in Fig. 6 illustrate that the calibration constants ( $V_0$  in Eq. 2) remained relatively stable (changes of 5% or less) for most AMODv2 units over the course of 15 months. However, several units  
 445 exhibited relatively large changes (in excess of 30%) in their calibration constants, indicating calibration changes may vary considerably by unit. Boersma and de Vroom (2005) present theoretical analyses and conclude that the calculation of AOD is most sensitive to errors in the calibration constant,  $V_0$ . (Boersma and de Vroom, 2006). Their

theoretical analyses combined with the results in Fig. 6, point to drift in  $V_0$  as a likely source for large, unit specific errors in AOD AMODv2 measurements. To limit errors due to calibration drift, we recommend that AMODv2  $V_0$  values be re-calibrated on an annual basis. Determining the source of changes to the calibration constants of some AMODv2 units is the subject of ongoing investigation. Potential sources include changes in sensitivity or drift of the photodiode sensor element, degrading of the optical interference filters, and/or clouding of the protective glass window element in the light path of the sensors.

### 3.3 Reliability testing

AMODv2 sensor validation results from this work and prior work indicate that the instrument can accurately measure AOD and PM2.5 when operating properly. However, for effective large-scale deployments, AMODv2 units must reliably complete their intended sampling protocol when deployed outdoors for 120 hours. Potential causes of premature sample failure included, premature battery drainage, damage to mechanical or electrical components (e.g. water ingress into motors or sensors), and firmware related crashes (e.g. memory overflow errors). In a series of reliability tests on the rooftop of our laboratory facility, we found that of 76 attempted samples, 75% were successfully completed, 16% failed due to premature battery drainage, 8% failed due to water damage, and 1% (one unit) failed due to a firmware crash. To address failures due to premature battery drainage, we replaced batteries that would not fully charge and replaced motors that were drawing excess current. To address failures due to water damage, we replaced damaged boards and applied additional sealant to key mechanical interfaces. We addressed the firmware crash issue by reconfiguring the memory allocation to grant more memory to the wireless data push functionality, which proved to be the most memory intensive sub-system. Overheating was not an issue in the testing discussed here, as the testing was conducted in winter months. We will test the AMODv2 under warmer conditions to evaluate heating effects on the performance of the instrument. We also verified that AMODv2 units were attempting AOD measurements and applying the prescribed data screening protocols. In the 76 test samples, AMODv2 units attempted 22,419 AOD measurements per wavelength. Units detected the sun and took at least one measurement toward forming a triplet 4,763 times per wavelength. The results partitioned by quality control designation are provided in Table 4. Instances where an AMODv2 reported a numerical AOD value were considered valid AOD measurements. Instances where an AMODv2 failed to acquire three AOD measurements for a single measurement sequence (Fig. S6) were designated as incomplete with a unique error code. Cloud-screened measurements were those where the solar alignment is achieved for 3 measurements but the triplet failed to meet the acceptance criteria (Fig. S6).

**Table 4: Results from the AMODv2 quality control algorithm from 4.763 AOD measurements taken in laboratory rooftop testing. Attempts where zero measurements were logged for a triplet attempt are omitted from the table.**

Wavelength (nm)	Proportion of valid AOD measurements	Proportion of invalid AOD measurements
-----------------	--------------------------------------	--

		Incomplete AOD triplets	Cloud-screened measurements
440	33%	20%	46%
500	34%	20%	45%
675	35%	20%	44%
870	33%	20%	46%

480

The results of this study indicate the AMODv2 automatically acquired solar alignment for a complete measurement triplet on 80% of attempted measurements. However, among the completed triplets, approximately 45% of measurements were identified as cloud-contaminated and subsequently screened. The screening algorithm did not reach consistent results across all wavelengths, as evident by slight deviations in the proportion of screened data across wavelengths. In this work, we applied the same exclusion criteria to each wavelength (Fig. S6). These results indicate unique exclusion criteria may be necessary for each wavelength to achieve consistent results, particularly when there is substantial deviation in magnitude between two measurement wavelengths (e.g. 440 nm AOD much higher than 870 nm AOD for a single measurement).

490 **Discussion and conclusions**

In the current study, we evaluated the AMODv2 under a wide range of atmospheric pollution levels and observed close agreement between the AMODv2 and AERONET AOD measurements, with mean absolute errors of 0.04, 0.06, 0.03, and 0.03 AOD units at 440 nm, 500 nm, 675 nm, and 870 nm, respectively. The agreement between AMODv2 and AERONET was stable across AOD levels ranging from  $0.016 \pm 0.01$  to  $1.590 \pm 0.01$ . We identified unit-specific changes to AOD calibration constants over time as a potential source of error in AOD measurements and recommended annual re-calibration (in line with recommendations for AERONET instruments) to mitigate those errors. While the AMODv2 was designed to be deployed by citizens, here the evaluation was done with data collected by team members. In Parts 1 and 2, we noted that there could be potential user errors that may impact the data quality. These were not analyzed in the present study. Even though the AMODv2 was designed to reduce these errors by automating the AOD process, there is still the potential for errors (i.e., improper placement). Future work describing the deployment of AMODv2s by citizen scientists should also include analysis of these issues.

The AMOD was designed to be a low-cost, user-friendly, and high-performance instrument for PM<sub>2.5</sub> and AOD measurements to be deployed in citizen-science campaigns. Citizen-led sampling is a promising approach to produce large-scale data sets to quantify air pollution concentrations at spatiotemporal resolution unachievable by more-expensive reference monitors (e.g., Brooks and Mims, 2001; Boersma and de Vroom, 2006; Ford et al., 2019). In Parts 1 and 2 of this series, we detailed the design and deployment of the AMODv1. In these previous studies, we noted several limitations of the instrument design that limited the amount of data (specifically AOD) collected by

505

participants. Here, we present the improvements made to the AMOD measurement system and the implementation of wireless data transfer and real-time visualization, which were the primary areas of improvement compared with the previous design. The new design of the AMODv2 allows for unsupervised measurement and quality control protocols that reduce the operational demands on a study volunteer, particularly compared with AMODv1 and other low-cost AOD sensors, while increasing the amount of data that can be collected. Deployments with citizen scientists are ongoing and data from those campaigns will be the subject of future studies. The portability, performance, and low cost of the AMODv2 make it a practical option to establish spatially-dense PM<sub>2.5</sub> and AOD measurement networks. Applied in these networks, the AMODv2 will close gaps in the existing global aerosol measurement infrastructure of ground-based and satellite-based observations.

*Data availability.*

All AMODv2 data collected and used in this study are available at the following URL:  
<https://hdl.handle.net/10217/225291>

*Supplement.*

The supplement related to this article is available online at:

*Author contributions.*

JV, JRP, SJ, ML, and BF designed the study and concept for which the AMODv2 was designed. EW, CQ, DML, CL, and JV designed the AMODv2 instrument. EW, CL, MC, and JM manufactured units. EW, BF, MC, ZR, CL, and JM designed validation experiments and analyzed validation data. CQ designed the mobile application. DHH developed the companion website. ZR, BF, ML, and EW wrote the user manual. EW led the paper with BF, JRP, SJ, and JV; and all co-authors contributed to interpretation of results and paper editing.

*Competing Interests.*

The authors declare that they have no conflict of interest.

*Acknowledgements.*

The authors wish to thank Mollie Phillips, Nick Trammel-Jamison, and Todd Hochwitz (Zebulon Solutions LLC, Longmont, CO, USA) for their contributions to this work. The authors also thank Michele Kuester of Digital Globe and Janae Csavina of NEON for their help securing AERONET co-location sites.

*Financial support.*

This research was supported by NASA grant 80NSSC18M0120.

## References

- Arku, R. E., Birch, A., Shupler, M., Yusuf, S., Hystad, P., and Brauer, M.: Characterizing exposure to household air pollution within the Prospective Urban Rural Epidemiology (PURE) study, *Environ. Int.*, 114, 307–317, <https://doi.org/10.1016/j.envint.2018.02.033>, 2018.
- 540 Badura, M., Sówka, I., Szymański, P., and Batog, P.: Assessing the usefulness of dense sensor network for PM<sub>2.5</sub> monitoring on an academic campus area, *Sci. Total Environ.*, 722, 137867, <https://doi.org/10.1016/j.scitotenv.2020.137867>, 2020.
- Bodhaine, B. A., Wood, N. B., Dutton, E. G., and Slusser, J. R.: On Rayleigh Optical Depth Calculations, *J. ATMOSPHERIC Ocean. Technol.*, 16, 8, 1999.
- 545 Boersma, K. F. and de Vroom, J. P.: Validation of MODIS aerosol observations over the Netherlands with GLOBE student measurements, *J. Geophys. Res.*, 111, D20311, <https://doi.org/10.1029/2006JD007172>, 2006.
- Brauer, M., Freedman, G., Frostad, J., van Donkelaar, A., Martin, R. V., Dentener, F., Dingenen, R. van, Estep, K., Amini, H., Apte, J. S., Balakrishnan, K., Barregard, L., Broday, D., Feigin, V., Ghosh, S., Hopke, P. K., Knibbs, L. D., Kokubo, Y., Liu, Y., Ma, S., Morawska, L., Sangrador, J. L. T., Shaddick, G., Anderson, H. R., Vos, T.,
- 550 Forouzanfar, M. H., Burnett, R. T., and Cohen, A.: Ambient Air Pollution Exposure Estimation for the Global Burden of Disease 2013, *Environ. Sci. Technol.*, 50, 79–88, <https://doi.org/10.1021/acs.est.5b03709>, 2016.
- Brooks, D. R. and Mims, F. M.: Development of an inexpensive handheld LED-based Sun photometer for the GLOBE program, *J. Geophys. Res. Atmospheres*, 106, 4733–4740, <https://doi.org/10.1029/2000JD900545>, 2001.
- Bulot, F. M. J., Johnston, S. J., Basford, P. J., Easton, N. H. C., Apetroaie-Cristea, M., Foster, G. L., Morris, A. K.
- 555 R., Cox, S. J., and Loxham, M.: Long-term field comparison of multiple low-cost particulate matter sensors in an outdoor urban environment, *Sci. Rep.*, 9, 7497, <https://doi.org/10.1038/s41598-019-43716-3>, 2019.
- Chadwick, E., Le, K., Pei, Z., Sayahi, T., Rapp, C., Butterfield, A. E., and Kelly, K. E.: Technical note: Understanding the effect of COVID-19 on particle pollution using a low-cost sensor network, *J. Aerosol Sci.*, 155, 105766, <https://doi.org/10.1016/j.jaerosci.2021.105766>, 2021.
- 560 Diner, D. J., Beckert, J. C., Reilly, T. H., Bruegge, C. J., Conel, J. E., Kahn, R. A., Martonchik, J. V., Ackerman, T. P., Davies, R., Gerstl, S. A. W., Gordon, H. R., Muller, J., Myneni, R. B., Sellers, P. J., Pinty, B., and Verstraete, M. M.: Multi-angle Imaging SpectroRadiometer (MISR) instrument description and experiment overview, *IEEE Trans. Geosci. Remote Sens.*, 36, 1072–1087, <https://doi.org/10.1109/36.700992>, 1998.
- van Donkelaar, A., Martin, R. V., and Park, R. J.: Estimating ground-level PM<sub>2.5</sub> using aerosol optical depth
- 565 determined from satellite remote sensing, *J. Geophys. Res.*, 111, D21201, <https://doi.org/10.1029/2005JD006996>, 2006.
- van Donkelaar, A., Martin, R. V., Brauer, M., Kahn, R., Levy, R., Verduzco, C., and Villeneuve, P. J.: Global Estimates of Ambient Fine Particulate Matter Concentrations from Satellite-Based Aerosol Optical Depth: Development and Application, *Environ. Health Perspect.*, 118, 847–855, <https://doi.org/10.1289/ehp.0901623>, 2010.
- 570 van Donkelaar, A., Martin, R. V., Pasch, A. N., Szykman, J. J., Zhang, L., Wang, Y. X., and Chen, D.: Improving the Accuracy of Daily Satellite-Derived Ground-Level Fine Aerosol Concentration Estimates for North America, *Environ. Sci. Technol.*, 46, 11971–11978, <https://doi.org/10.1021/es3025319>, 2012.

van Donkelaar, A., Martin, R. V., Brauer, M., Hsu, N. C., Kahn, R. A., Levy, R. C., Lyapustin, A., Sayer, A. M., and Winker, D. M.: Global Estimates of Fine Particulate Matter using a Combined Geophysical-Statistical Method with Information from Satellites, Models, and Monitors, *Environ. Sci. Technol.*, 50, 3762–3772, <https://doi.org/10.1021/acs.est.5b05833>, 2016.

van Donkelaar, A., Martin, R. V., Li, C., and Burnett, R. T.: Regional Estimates of Chemical Composition of Fine Particulate Matter Using a Combined Geoscience-Statistical Method with Information from Satellites, Models, and Monitors, *Environ. Sci. Technol.*, 53, 2595–2611, <https://doi.org/10.1021/acs.est.8b06392>, 2019.

Feng, S., Gao, D., Liao, F., Zhou, F., and Wang, X.: The health effects of ambient PM<sub>2.5</sub> and potential mechanisms, *Ecotoxicol. Environ. Saf.*, 128, 67–74, <https://doi.org/10.1016/j.ecoenv.2016.01.030>, 2016.

Ford, B. and Heald, C. L.: Exploring the uncertainty associated with satellite-based estimates of premature mortality due to exposure to fine particulate matter, *Atmospheric Chem. Phys.*, 16, 3499–3523, <https://doi.org/10.5194/acp-16-3499-2016>, 2016.

Ford, B., Pierce, J. R., Wendt, E., Long, M., Jathar, S., Mehaffy, J., Tryner, J., Quinn, C., van Zyl, L., L’Orange, C., Miller-Lionberg, D., and Volckens, J.: A low-cost monitor for measurement of fine particulate matter and aerosol optical depth – Part 2: Citizen-science pilot campaign in northern Colorado, *Atmospheric Meas. Tech.*, 12, 6385–6399, <https://doi.org/10.5194/amt-12-6385-2019>, 2019.

Forouzanfar, M. H., Afshin, A., Alexander, L. T., Anderson, H. R., Bhutta, Z. A., Biryukov, S., Brauer, M., Burnett, R., Cercy, K., Charlson, F. J., Cohen, A. J., Dandona, L., Estep, K., Ferrari, A. J., Frostad, J. J., Fullman, N., Gething, P. W., Godwin, W. W., Griswold, M., Hay, S. I., Kinfu, Y., Kyu, H. H., Larson, H. J., Liang, X., Lim, S. S., Liu, P. Y., Lopez, A. D., Lozano, R., Marczak, L., Mensah, G. A., Mokdad, A. H., Moradi-Lakeh, M., Naghavi, M., Neal, B., Reitsma, M. B., Roth, G. A., Salomon, J. A., Sur, P. J., Vos, T., Wagner, J. A., Wang, H., Zhao, Y., Zhou, M., Aasvang, G. M., Abajobir, A. A., Abate, K. H., Abbafati, C., Abbas, K. M., Abd-Allah, F., Abdulle, A. M., Abera, S. F., Abraham, B., Abu-Raddad, L. J., Abyu, G. Y., Adebisi, A. O., Adedeji, I. A., Ademi, Z., Adou, A. K., Adsuar, J. C., Agardh, E. E., Agarwal, A., Agrawal, A., Kiadaliri, A. A., Ajala, O. N., Akinyemiju, T. F., Al-Aly, Z., Alam, K., Alam, N. K. M., Aldhahri, S. F., Aldridge, R. W., Alemu, Z. A., Ali, R., Alkerwi, A., Alla, F., Allebeck, P., Alsharif, U., Altirkawi, K. A., Martin, E. A., Alvis-Guzman, N., Amare, A. T., Amberbir, A., Amegah, A. K., Amini, H., Ammar, W., Amrock, S. M., Andersen, H. H., Anderson, B. O., Antonio, C. A. T., Anwari, P., Ärnlöv, J., Artaman, A., Asayesh, H., Asghar, R. J., Assadi, R., Atique, S., Avokpaho, E. F. G. A., Awasthi, A., Quintanilla, B. P. A., Azzopardi, P., et al.: Global, regional, and national comparative risk assessment of 79 behavioural, environmental and occupational, and metabolic risks or clusters of risks, 1990–2015: a systematic analysis for the Global Burden of Disease Study 2015, *The Lancet*, 388, 1659–1724, [https://doi.org/10.1016/S0140-6736\(16\)31679-8](https://doi.org/10.1016/S0140-6736(16)31679-8), 2016.

Garay, M. J., Kalashnikova, O. V., and Bull, M. A.: Development and assessment of a higher-spatial-resolution (4.4 km) MISR aerosol optical depth product using AERONET-DRAGON data, *Atmospheric Chem. Phys.*, 17, 5095–5106, <https://doi.org/10.5194/acp-17-5095-2017>, 2017.

Giles, D. M., Sinyuk, A., Sorokin, M. G., Schafer, J. S., Smirnov, A., Slutsker, I., Eck, T. F., Holben, B. N., Lewis, J. R., Campbell, J. R., Welton, E. J., Korkin, S. V., and Lyapustin, A. I.: Advancements in the Aerosol Robotic

- 610 Network (AERONET) Version 3 database – automated near-real-time quality control algorithm with improved cloud screening for Sun photometer aerosol optical depth (AOD) measurements, *Atmospheric Meas. Tech.*, 12, 169–209, <https://doi.org/10.5194/amt-12-169-2019>, 2019.
- Griggs, M.: Absorption Coefficients of Ozone in the Ultraviolet and Visible Regions, *J. Chem. Phys.*, 49, 857–859, <https://doi.org/10.1063/1.1670152>, 1968.
- 615 Hammer, M. S., van Donkelaar, A., Li, C., Lyapustin, A., Sayer, A. M., Hsu, N. C., Levy, R. C., Garay, M. J., Kalashnikova, O. V., Kahn, R. A., Brauer, M., Apte, J. S., Henze, D. K., Zhang, L., Zhang, Q., Ford, B., Pierce, J. R., and Martin, R. V.: Global Estimates and Long-Term Trends of Fine Particulate Matter Concentrations (1998–2018), *Environ. Sci. Technol.*, 54, 7879–7890, <https://doi.org/10.1021/acs.est.0c01764>, 2020.
- Holben, B. N., Eck, T. F., Slutsker, I., Tanré, D., Buis, J. P., Setzer, A., Vermote, E., Reagan, J. A., Kaufman, Y. J., 620 Nakajima, T., Lavenu, F., Jankowiak, I., and Smirnov, A.: AERONET—A Federated Instrument Network and Data Archive for Aerosol Characterization, *Remote Sens. Environ.*, 66, 1–16, [https://doi.org/10.1016/S0034-4257\(98\)00031-5](https://doi.org/10.1016/S0034-4257(98)00031-5), 1998.
- Janssen, N. A. H., Fischer, P., Marra, M., Ameling, C., and Cassee, F. R.: Short-term effects of PM<sub>2.5</sub>, PM<sub>10</sub> and PM<sub>2.5–10</sub> on daily mortality in the Netherlands, *Sci. Total Environ.*, 463–464, 20–26, 625 <https://doi.org/10.1016/j.scitotenv.2013.05.062>, 2013.
- Jin, X., Fiore, A. M., Curci, G., Lyapustin, A., Civerolo, K., Ku, M., van Donkelaar, A., and Martin, R. V.: Assessing uncertainties of a geophysical approach to estimate surface fine particulate matter distributions from satellite-observed aerosol optical depth, *Atmospheric Chem. Phys.*, 19, 295–313, <https://doi.org/10.5194/acp-19-295-2019>, 2019.
- 630 Kelleher, S., Quinn, C., Miller-Lionberg, D., and Volckens, J.: A low-cost particulate matter (PM<sub>2.5</sub>) monitor for wildland fire smoke, *Atmospheric Meas. Tech.*, 11, 1087–1097, <https://doi.org/10.5194/amt-11-1087-2018>, 2018.
- Kelly, K. E., Whitaker, J., Petty, A., Widmer, C., Dybwad, A., Sleeth, D., Martin, R., and Butterfield, A.: Ambient and laboratory evaluation of a low-cost particulate matter sensor, *Environ. Pollut.*, 221, 491–500, <https://doi.org/10.1016/j.envpol.2016.12.039>, 2017.
- 635 Kim, I., Lee, K., Lee, S., and Kim, S. D.: Characteristics and health effects of PM<sub>2.5</sub> emissions from various sources in Gwangju, South Korea, *Sci. Total Environ.*, 696, 133890, <https://doi.org/10.1016/j.scitotenv.2019.133890>, 2019.
- Lee, C.: Impacts of multi-scale urban form on PM<sub>2.5</sub> concentrations using continuous surface estimates with high-resolution in U.S. metropolitan areas, *Landsc. Urban Plan.*, 204, 103935, <https://doi.org/10.1016/j.landurbplan.2020.103935>, 2020.
- 640 Levy Zamora, M., Xiong, F., Gentner, D., Kerkez, B., Kohnman-Glaser, J., and Koehler, K.: Field and Laboratory Evaluations of the Low-Cost Plantower Particulate Matter Sensor, *Environ. Sci. Technol.*, 53, 838–849, <https://doi.org/10.1021/acs.est.8b05174>, 2019.
- Li, J., Liu, H., Lv, Z., Zhao, R., Deng, F., Wang, C., Qin, A., and Yang, X.: Estimation of PM<sub>2.5</sub> mortality burden in China with new exposure estimation and local concentration-response function, *Environ. Pollut.*, 243, 1710–1718, 645 <https://doi.org/10.1016/j.envpol.2018.09.089>, 2018.
- Li, J., Zhang, H., Chao, C.-Y., Chien, C.-H., Wu, C.-Y., Luo, C. H., Chen, L.-J., and Biswas, P.: Integrating low-

cost air quality sensor networks with fixed and satellite monitoring systems to study ground-level PM<sub>2.5</sub>, *Atmos. Environ.*, 223, 117293, <https://doi.org/10.1016/j.atmosenv.2020.117293>, 2020.

650 Lin, C., Labzovskii, L. D., Leung Mak, H. W., Fung, J. C. H., Lau, A. K. H., Kenea, S. T., Bilal, M., Vande Hey, J. D., Lu, X., and Ma, J.: Observation of PM<sub>2.5</sub> using a combination of satellite remote sensing and low-cost sensor network in Siberian urban areas with limited reference monitoring, *Atmos. Environ.*, 227, 117410, <https://doi.org/10.1016/j.atmosenv.2020.117410>, 2020.

655 Liu, Y., Sarnat, J. A., Kilaru, V., Jacob, D. J., and Koutrakis, P.: Estimating Ground-Level PM<sub>2.5</sub> in the Eastern United States Using Satellite Remote Sensing, *Environ. Sci. Technol.*, 39, 3269–3278, <https://doi.org/10.1021/es049352m>, 2005.

Lu, X., Lin, C., Li, W., Chen, Y., Huang, Y., Fung, J. C. H., and Lau, A. K. H.: Analysis of the adverse health effects of PM<sub>2.5</sub> from 2001 to 2017 in China and the role of urbanization in aggravating the health burden, *Sci. Total Environ.*, 652, 683–695, <https://doi.org/10.1016/j.scitotenv.2018.10.140>, 2019.

660 Lu, Y., Giuliano, G., and Habre, R.: Estimating hourly PM<sub>2.5</sub> concentrations at the neighborhood scale using a low-cost air sensor network: A Los Angeles case study, *Environ. Res.*, 195, 110653, <https://doi.org/10.1016/j.envres.2020.110653>, 2021.

665 Myhre, G., Shindell, D., Bréon, F.-M., Collins, W., Fuglestedt, J., Huang, J., Koch, D., Lamarque, J.-F., Lee, D., Mendoza, B., Nakajima, T., Robock, A., Stephens, G., Zhang, H., Aamaas, B., Boucher, O., Dalsøren, S. B., Daniel, J. S., Forster, P., Granier, C., Haigh, J., Hodnebrog, Ø., Kaplan, J. O., Marston, G., Nielsen, C. J., O'Neill, B. C., Peters, G. P., Pongratz, J., Ramaswamy, V., Roth, R., Rotstayn, L., Smith, S. J., Stevenson, D., Vernier, J.-P., Wild, O., Young, P., Jacob, D., Ravishankara, A. R., and Shine, K.: 8 Anthropogenic and Natural Radiative Forcing, 82, 2013.

670 Pillarisetti, A., Carter, E., Rajkumar, S., Young, B. N., Benka-Coker, M. L., Peel, J. L., Johnson, M., and Clark, M. L.: Measuring personal exposure to fine particulate matter (PM<sub>2.5</sub>) among rural Honduran women: A field evaluation of the Ultrasonic Personal Aerosol Sampler (UPAS), *Environ. Int.*, 123, 50–53, <https://doi.org/10.1016/j.envint.2018.11.014>, 2019.

Pope, C. A. and Dockery, D. W.: Health Effects of Fine Particulate Air Pollution: Lines that Connect, *J. Air Waste Manag. Assoc.*, 56, 709–742, <https://doi.org/10.1080/10473289.2006.10464485>, 2006.

675 Reda, I. and Andreas, A.: Solar Position Algorithm for Solar Radiation Applications (Revised), <https://doi.org/10.2172/15003974>, 2008.

Salomonson, V. V., Barnes, W. L., Maymon, P. W., Montgomery, H. E., and Ostrow, H.: MODIS: advanced facility instrument for studies of the Earth as a system, *IEEE Trans. Geosci. Remote Sens.*, 27, 145–153, <https://doi.org/10.1109/36.20292>, 1989.

680 Sayahi, T., Butterfield, A., and Kelly, K. E.: Long-term field evaluation of the Plantower PMS low-cost particulate matter sensors, *Environ. Pollut.*, 245, 932–940, <https://doi.org/10.1016/j.envpol.2018.11.065>, 2019.

Sayer, A. M., Hsu, N. C., Bettenhausen, C., Jeong, M.-J., Holben, B. N., and Zhang, J.: Global and regional evaluation of over-land spectral aerosol optical depth retrievals from SeaWiFS, *Atmospheric Meas. Tech.*, 5, 1761–1778, <https://doi.org/10.5194/amt-5-1761-2012>, 2012.

Smirnov, A., Holben, B. N., Eck, T. F., Dubovik, O., and Slutsker, I.: Cloud-Screening and Quality Control Algorithms for the AERONET Database, *Remote Sens. Environ.*, 73, 337–349, [https://doi.org/10.1016/S0034-4257\(00\)00109-7](https://doi.org/10.1016/S0034-4257(00)00109-7), 2000.

Snider, G., Weagle, C. L., Martin, R. V., van Donkelaar, A., Conrad, K., Cunningham, D., Gordon, C., Zwicker, M., Akoshile, C., Artaxo, P., Anh, N. X., Brook, J., Dong, J., Garland, R. M., Greenwald, R., Griffith, D., He, K., Holben, B. N., Kahn, R., Koren, I., Lagrosas, N., Lestari, P., Ma, Z., Vanderlei Martins, J., Quel, E. J., Rudich, Y., Salam, A., Tripathi, S. N., Yu, C., Zhang, Q., Zhang, Y., Brauer, M., Cohen, A., Gibson, M. D., and Liu, Y.: SPARTAN: a global network to evaluate and enhance satellite-based estimates of ground-level particulate matter for global health applications, *Atmospheric Meas. Tech.*, 8, 505–521, <https://doi.org/10.5194/amt-8-505-2015>, 2015.

Tryner, J., L’Orange, C., Mehaffy, J., Miller-Lionberg, D., Hofstetter, J. C., Wilson, A., and Volckens, J.: Laboratory evaluation of low-cost PurpleAir PM monitors and in-field correction using co-located portable filter samplers, *Atmos. Environ.*, 220, 117067, <https://doi.org/10.1016/j.atmosenv.2019.117067>, 2020.

Van Heuklon, T. K.: Estimating atmospheric ozone for solar radiation models, *Sol. Energy*, 22, 63–68, [https://doi.org/10.1016/0038-092X\(79\)90060-4](https://doi.org/10.1016/0038-092X(79)90060-4), 1979.

Vohra, K., Vodonos, A., Schwartz, J., Marais, E. A., Sulprizio, M. P., and Mickley, L. J.: Global mortality from outdoor fine particle pollution generated by fossil fuel combustion: Results from GEOS-Chem, *Environ. Res.*, 195, 110754, <https://doi.org/10.1016/j.envres.2021.110754>, 2021.

Volckens, J., Quinn, C., Leith, D., Mehaffy, J., Henry, C. S., and Miller-Lionberg, D.: Development and evaluation of an ultrasonic personal aerosol sampler, *Indoor Air*, 27, 409–416, <https://doi.org/10.1111/ina.12318>, 2017.

Wendt, E. A., Quinn, C. W., Miller-Lionberg, D. D., Tryner, J., L’Orange, C., Ford, B., Yalin, A. P., Pierce, J. R., Jathar, S., and Volckens, J.: A low-cost monitor for simultaneous measurement of fine particulate matter and aerosol optical depth – Part 1: Specifications and testing, *Atmospheric Meas. Tech.*, 12, 5431–5441, <https://doi.org/10.5194/amt-12-5431-2019>, 2019.

Young, A. T.: Air mass and refraction, *Appl. Opt.*, 33, 1108, <https://doi.org/10.1364/AO.33.001108>, 1994.

Zheng, T., Bergin, M. H., Johnson, K. K., Tripathi, S. N., Shirodkar, S., Landis, M. S., Sutaria, R., and Carlson, D. E.: Field evaluation of low-cost particulate matter sensors in high- and low-concentration environments, *Atmospheric Meas. Tech.*, 11, 4823–4846, <https://doi.org/10.5194/amt-11-4823-2018>, 2018.